*molecules*

MDPI

*Article*

# Theoretical Insight into the Reaction Mechanism and Kinetics for the Criegee Intermediate of *anti*-PhCHOO with $SO_2$

**Benni Du and Weichao Zhang ***

School of Chemistry and Materials Science, Jiangsu Normal University, Xuzhou 221116, Jiangsu, China; dubn@jsnu.edu.cn

* Correspondence: zwc@jsnu.edu.cn; Tel.: +86-516-8340-3165; Fax: +86-516-8340-3164

Received: 15 June 2020; Accepted: 2 July 2020; Published: 3 July 2020


**Abstract:** In this study, the density functional theory (DFT) and CCSD(T) method have been performed to gain insight into the possible products and detailed reaction mechanism of the Criegee intermediate (CI) of *anti*-PhCHOO with $SO_2$ for the first time. The potential energy surfaces (PESs) have been depicted at the UCCSD(T)/6-311++G(d,p)//UB3LYP/6-311++G(d,p) levels of theory with ZPE correction. Two different five-membered ring adducts, viz., *endo* PhCHOOS(O)O (IM1) and *exo* PhCHOOS(O)O (IM2) have been found in the entrance of reaction channels. Both direct and indirect reaction pathways from IM1 and IM2 have been considered for the title reaction. Our calculations show that the formation of PhCHO+$SO_3$ (P1) via indirect reaction pathways from IM1 is predominant in all the pathways, and the production of P1 via direct dissociation pathway of IM1 and indirect reaction pathways of IM2 cannot be neglected. Moreover, PhCOOH+$SO_2$ (P2) initiated from IM2 is identified as the minor product. According to the kinetic calculation, the total rate constant for the *anti*-PhCHOO+$SO_2$ reaction is estimated to be $6.98 \times 10^{-10}$ $cm^3 \cdot molecule^{-1} \cdot s^{-1}$ at 298 K.

**Keywords:** Criegee intermediate; *anti*-PhCHOO; product distribution; kinetic calculation

## 1. Introduction

Criegee intermediate (CI) is an important species formed in the ozonolysis of alkenes, and it is a carbonyl oxide with diradical electronic structure [1]. Since the first direct observation [2] and direct kinetic measurements [3] for the simplest CI, $CH_2OO$, recently, much attention has been given to the reactions of CIs in atmospheric chemistry. Due to the significance in ozonolysis mechanism and possessing high reactivity, it has been suggested that CIs can be added as a new type of atmospheric active species in atmospheric oxidation chemistry, besides OH, $NO_3$, and $O_3$ et al. [4].

When released into the atmosphere, the CIs can react with some atmospheric species, such as $H_2O$ [3,5–14], $HO_2$ [15,16], $NO_2$ [3,10,17–19], $SO_2$ [3,9–11,14,19–29], OH [30] and $CH_2$=C($CH_3$)CHO [31] et al., to form corresponding products. The reactions of CIs with $SO_2$ in particular play an important role in atmospheric chemistry, due to the formation of $SO_3$ and subsequent $H_2SO_4$, which is the main component of aerosols and acid rain [32–35], and this provides another feasible channel for the formation of $H_2SO_4$ in the atmosphere.

For the reactions of CIs with $SO_2$, many experimental and theoretical studies have been carried out to investigate the kinetics and reaction mechanism for the simplest $CH_2OO$ [3,5,9–11,20–25,31], *anti*- or *syn*-$CH_3CHOO$ and $(CH_3)_2COO$ [11,19,21,22,24,26–28,30]. Moreover, the reactions of $SO_2$ with those CIs produced from czonolysis of limonene, α- pinene, β-pinene [20,29], and styrene [14] etc., have also been studied to investigate the influence of these reactions of CIs+$SO_2$ to the formation of sulfuric acid or the secondary aerosols.

In 2017, Díaz-de-Mera et al. [14] studied the ozonolysis of styrene in the presence of $SO_2$ at atmospheric pressure and room temperature. The formation of $SO_3$ is expected to be major in reaction of Criegee intermediates with $SO_2$. They found that lower concentrations of reactants were required in the ozonolysis of styrene with low concentrations of $SO_2$ than those required in experiments without $SO_2$. Furthermore, under high $H_2O$ concentrations, the formation of $SO_3$ and subsequent $H_2SO_4$ in the smog chamber is inhibited, due to the competitive reactions of CIs with water. However, the rate constants ratio of $(2.8 \pm 0.7) \times 10^{-5}$ (errors are $2\sigma \pm 20\%$) for $k(H_2O)/k(SO_2)$ illustrates that the reaction of CIs with $SO_2$ will be fast under atmospheric conditions.

In the ozonolysis of styrene, both $CH_2OO$ and $C_6H_5CHOO$ (denoted as PhCHOO) will be formed. For the case of $CH_2OO$, the reactions with $SO_2$ have been studied extensively [3,5,9–11,20–25,31], both in experiment and theory, while for the reaction of PhCHOO+$SO_2$, as far as we know, no corresponding theoretical study has been done. Thus, the main goal of this work is to explore the reaction mechanism and kinetics of *anti*-PhCHOO+$SO_2$, give the possible product channels, and compare with the available experimental results. The proposed reaction pathways for the reaction of *anti*-PhCHOO+$SO_2$ are presented in Scheme 1.

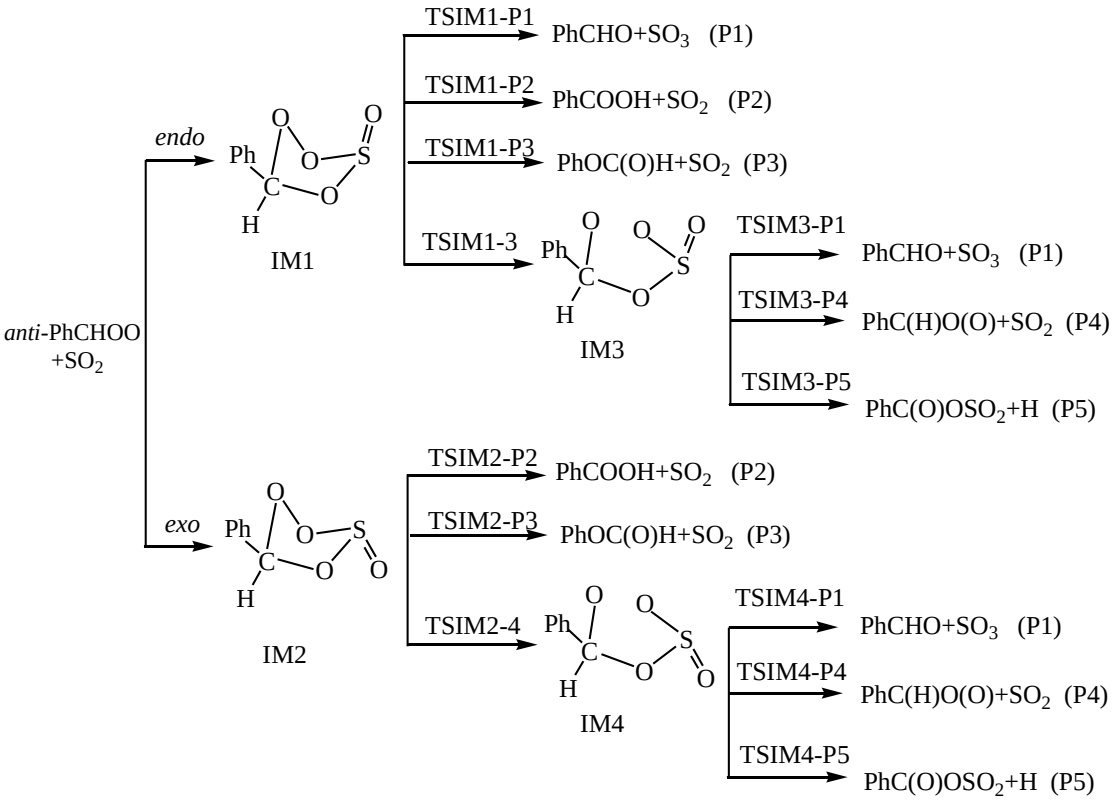


**Scheme 1.** Proposed mechanisms for the *anti*-PhCHOO+$SO_2$ reactions.

## 2. Computational Method

The Gaussian 09 package [36] was used to all ab initio calculations. Due to the ability of accurate describing the geometries of transition states and providing some properties that can be comparable in accuracy to higher levels of theory, the hybrid B3LYP [37,38] method has been employed extensively in the CI reaction systems [5,7,13,20,21,24], thus, the geometries of all species involved in the title reaction have been optimized at the B3LYP/6-311++G(d,p) level of theory. Harmonic vibrational frequency calculations were performed at the same level of theory to confirm the character of each stationary point, i.e., all real frequencies for a minimum and only one imaginary frequency for a transition state structure. Moreover, zero-point vibrational energy (ZPE) correction was also obtained from such calculations. Intrinsic reaction coordinate (IRC) [39,40] calculations were also carried

out, to verify the connectivity of the transition state structures. To obtain more reliable relative energies, single-point energies of all stationary points at the B3LYP/6-311++G(d,p) geometries were calculated using coupled-cluster theory including single, double, and noniterative triple excitations [CCSD(T)] [41] using the 6-311++G(d,p) basis set. The ZPE corrections with a scale factor of 0.9688 [42] were included in the determination of energy barriers and reaction energies. We noted that the B3LYP/6-311++G(d,p) calculations were unable to locate the reactant complexes RC1, RC2, and transition states TSRC1-1, TSRC2-2 in the entrance channels. However, they could be obtained using the BH&HLYP method [38,43]. Therefore, the stationary points of RC1, RC2, TSRC1-1, and TSRC2-2 were reoptimized at the BH&HLYP/6-311++G(d,p) level. The single-point energy of each optimized geometry at the BH&LYP/6-311++G(d,p) level was recalculated, using the CCSD(T)/6-311++G(d,p) level of theory, with the ZPE correction scaled by 0.9335 [42]. Here, we would like to explain that how the ZPE correction obtained by the DFT method is transformed into the one obtained by the CCSD(T) method. The PESs obtained at 0 K are useful for kinetic analysis, especially for the rate constant calculation at different temperatures. The reliable energies at 0 K of all stationary points can be determined directly by geometry optimization and frequency calculation, using the CCSD(T) method. However, the geometry optimization and frequency calculations at CCSD(T) method are very expensive indeed. In general, the CCSD(T) total energy at 0 K is obtained by adding the DFT-determined ZPE correction to the CCSD(T) single point energy on the basis of DFT geometry optimization. This method is widely used in the PESs construction of reaction systems [44,45]. Moreover, due to the neglection of anharmonicity effects in the theoretical treatment, incomplete incorporation of electron correlation, and the use of finite basis sets, the computed quantum chemical harmonic vibrational frequencies are typically larger than the fundamentals observed experimentally. Therefore, the frequency scale factors are applied to obtain fundamentals and ZPEs [42].

It should be pointed out that, due to the special singlet diradical structure, the closed-shell paradigm is not suitable to CIs. Thus, similar to the reaction of $CH_2OO$+$SO_2$ [23], the unrestricted broken symmetry approach—mixing the highest occupied molecular orbital (HOMO) and lowest unoccupied molecular orbital (LUMO) option proposed by Noodleman [46]—was used for these species in the geometry optimizations and single-point energies calculations. Moreover, the %TAE[(T)] diagnostic method was used to estimate the magnitude of post-CCSD(T) contributions. It has been shown that %TAE[(T)] diagnostic can provide a useful a priori indicator of the magnitude of the post-CCSD(T) contributions to the total atomization energies (TAEs) [47,48]. According to the %TAE[(T)] values, (%TAE[(T)] = 100 × (TAE[CCSD(T)]−TAE[CCSD])/TAE[CCSD(T)], we can see from Table S1 of Supplementary Materials that all the %TAE[(T)] diagnostic values are small (below 0.02%), which suggests that the post-CCSD(T) contributions should not exceed 0.5 kcal/mol [48], and the application of CCSD(T)/6-311++G(d,p) for this system is suitable.

## 3. Results and Discussion

### *3.1. Reaction Mechanism*

In the ozonolysis of styrene, both *syn*- and *anti*- PhCHOO will be formed in the initial steps. The *anti*-PhCHOO species has a smaller steric hindrance than *syn*-PhCHOO in the formation of the corresponding complexes and (or) adducts when drawing near $SO_2$, as illustrated in the similar reactions of *anti*-$CH_3CHOO$ with $H_2O$ [8] and $SO_2$ [26] etc., thus, only the *anti*-PhCHOO conformer is selected as the initial reactant.

The optimized geometries and critical structural parameters for various species, including reactants, reactant complexes (RC), intermediates (IM), transition states (TS), and products associated with the reaction of *anti*-PhCHOO with $SO_2$ are shown in Figure S1, Figure S2, and Figure S3 of the Supplementary Materials. In Table S2 of the Supplementary Materials, the ZPE, total energies, and relative energies (relative to the isolated species) without and with ZPE corrections of all stationary

points calculated at the UCCSD(T)/6-311++G(d,p)//UB3LYP/6-311++G(d,p) levels of theory with ZPE corrections (denoted as UCCSD(T)//UB3LYP) are listed.

The potential energy surfaces (PESs) for the reaction of *anti*-PhCHOO+$SO_2$ plotted by the relative energies are shown in Figures 1 and 2, together with the labeling of atoms in the reactant complexes.

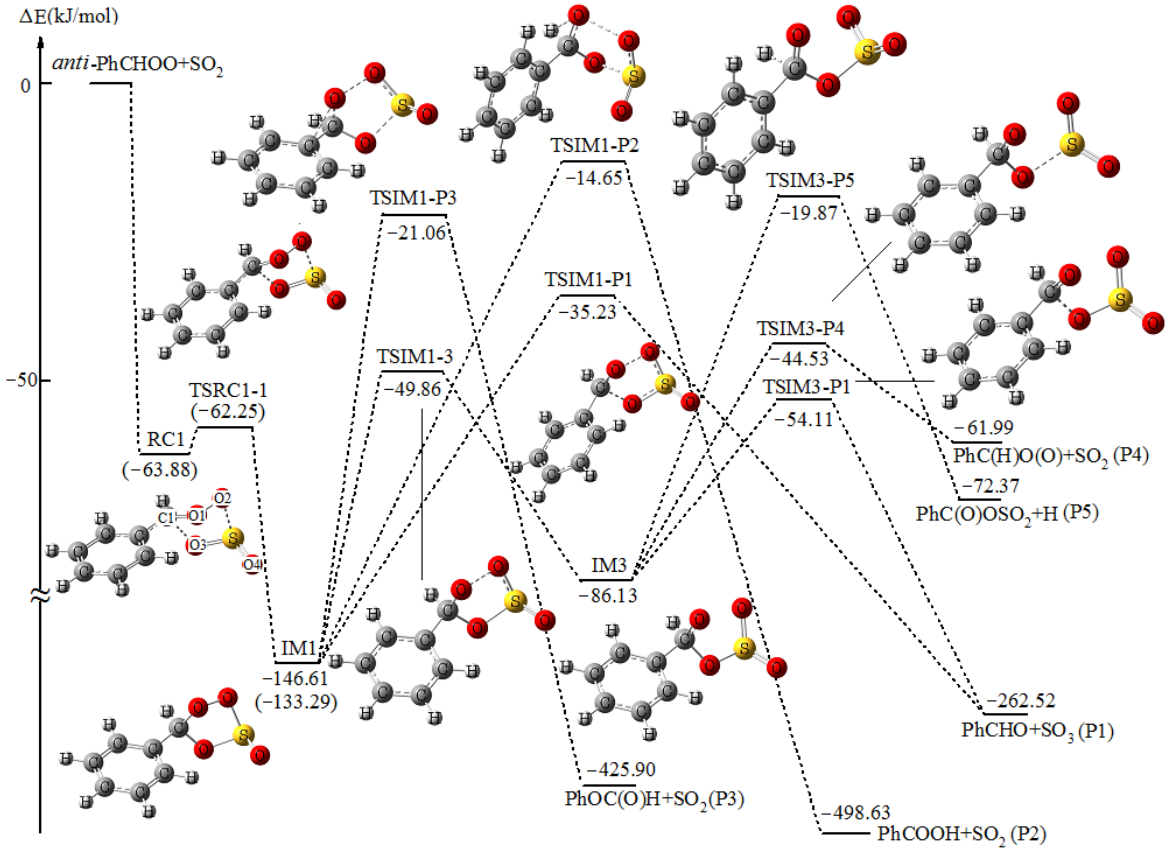


**Figure 1.** Potential energy profile for the formation and subsequent reaction pathways of *endo* PhCHOOS(O)O (IM1) in the reaction of *anti*-PhCHOO+$SO_2$ at the UCCSD(T)//UB3LYP level with zero-point vibrational energy (ZPE) corrections. The values in parentheses are derived from UCCSD(T)//UBH&HLYP level with ZPE corrections.

Similar to other CIs, the *anti*-PhCHOO produced in the ozonolysis of styrene is highly reactive, and it can be stabilized by collision, followed by the reaction with $SO_2$, to form corresponding products.

As shown in Figures 1 and 2, with the approach of $SO_2$ from different directions, the reaction can proceed through the formation of two reactant complexes RC1 and RC2 in the entrance channels. Subsequently, with the S atom of $SO_2$ bonding to the CI terminal O2 atom and the O3 atom of $SO_2$ bonding to the C atom of CI simultaneously, two cyclic adducts *endo* PhCHOOS(O)O (IM1) and *exo* PhCHOOS(O)O (IM2) will be formed via TSRC1-1 and TSRC2-2, respectively. It has been mentioned in the Computational Method section that, at the B3LYP level, no corresponding reactant complexes and transition states have been found in the formation of IM1 and IM2, despite numerous attempts. The structures and energies of RC1, RC2, TSRC1-1, and TSRC2-2 shown in Figures 1 and 2 are obtained at the UBH&HLYP/6-311++G(d,p) and UCCSD(T)/6-311++G(d,p)//UBH&HLYP/6-311++G(d,p), with ZPE corrections (denoted as UCCSD(T)//UBH&HLYP), levels of theory, respectively. The relative energies of RC1 and RC2 are −63.88 and −68.93 kJ/mol, and the corresponding transition states TSRC1-1 and TSRC2-2 lie slightly higher (1.63 kJ/mol for TSRC1-1), or even lower (−0.15 kJ/mol for TSRC2-2) than that of RC1 and RC2, respectively. Obviously, the formation of reactant complexes RC1 and RC2 and the subsequent adducts IM1 and IM2 is (or almost) barrierless. These results can find support

from the frontier orbital analysis. As shown in Figure 3, at the UBH&HLYP/6-311++G(d,p) level, the electron density distribution localized on the fragment of –CHOO in the HOMO of *anti*-PhCHOO and the LUMO of $SO_2$ is symmetry matching. Furthermore, the energy difference of 0.18539 a.u. between the HOMO of *anti*-PhCHOO and the LUMO of $SO_2$ is smaller than 0.34151 a.u. between the HOMO of $SO_2$ and the LUMO of *anti*-PhCHOO, thus, the reaction can proceed without barriers via interaction between the HOMO of *anti*-PhCHOO and the LUMO of $SO_2$, to form RC1 and RC2.

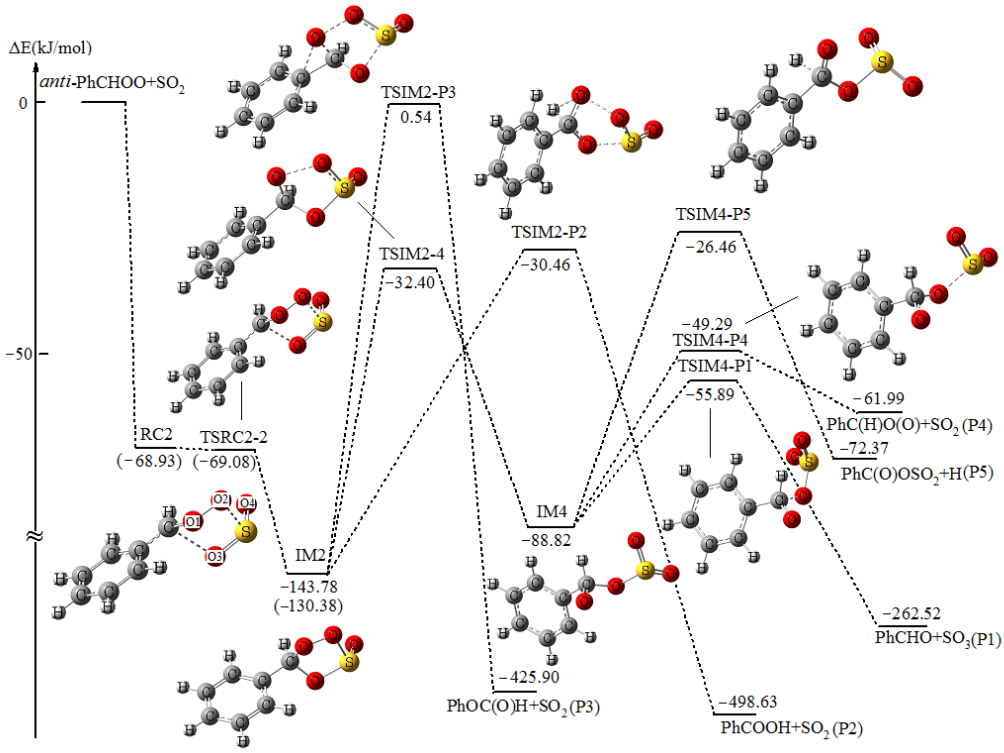


**Figure 2.** Potential energy profile for the formation and subsequent reaction pathways of *exo* PhCHOOS(O)O (IM2) in the reaction of *anti*-PhCHOO+$SO_2$ at the UCCSD(T)//UB3LYP level with ZPE corrections. The values in parentheses are derived from UCCSD(T)//UBH&HLYP level with ZPE corrections.

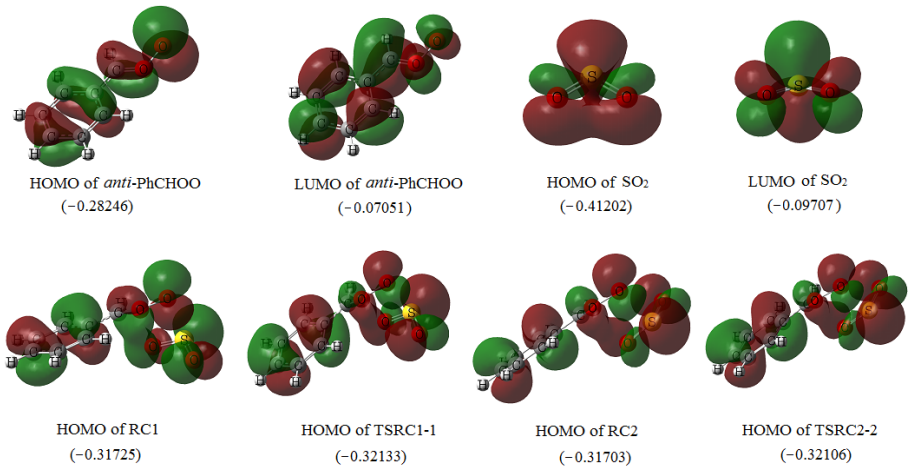


**Figure 3.** Highest occupied molecular orbital (HOMO) and lowest unoccupied molecular orbital (LUMO) orbital pictures of *anti*-PhCHOO and $SO_2$, together with the HOMO of reactant complexes (RC)1, TSRC1-1, RC2 and TSRC2-2. The values in parentheses are the orbital energies (a.u.) calculated at the UBH&HLYP/6-311++G(d,p) level.

Comparing the HOMO of RC1 with that of TSRC1-1 shown in Figure 3, we can see that they have similar electronic density distribution and approximate orbital energies, that is to say, from RC1 to TSRC1-1, there is no obvious change of electron density distribution, which results in the formation of IM1 with almost no barrier. The similar instance can also be derived in the formation of IM2, according to the electronic density distribution in the HOMO of RC2 and TSRC2-2.

As depicted in Figures 1 and 2, IM1 and IM2 are a pair of conformational isomers with the S=O double bond pointing to the outside and inside the plane, respectively. IM1 and IM2 lie 146.61 and 143.78 kJ/mol below the initial reactants, and this suggests that they have enough internal energy for the subsequent reactions.

Both isomerization and dissociation pathways of IM1 and IM2 have been considered, and they are discussed as follows.

Firstly, with the simultaneous fracture of O1-O2 and C-O3 bonds initiated from IM1, the products of benzaldehyde (PhCHO)+$SO_3$ (P1) will be formed via the transition state TSIM1-P1, by overcoming a barrier of 111.38 kJ/mol.

Secondly, when the H atom shifting from the C1 atom to the adjacent O1 atom, the $SO_2$ fragment (O2-S-O4) is also departed from the parent molecule via transition state TSIM1-P2, to produce benzoic acid (PhCOOH). The relative energy of TSIM1-P2 is -14.65 kJ/mol and it is 20.58 kJ/mol higher than that TSIM1-P1. Obviously, the production of P1 is more favorable than that of PhCOOH+$SO_2$ (P2), due to its lower energy barrier.

The formation of singlet bisoxy diradical PhC(H)O(O) has also been considered, starting from IM1. However, an attempt to locate the corresponding TS at the B3LYP level was not successful. With the departure of $SO_2$ via breaking the O1-O2 and S-O3 bonds, the product of phenyl formate (PhOC(O)H) will be formed via TSIM1-P3 after climbing the barrier height of 125.55 kJ/mol. The IRC analysis of TSIM1-P3 shown in Figure S4 verifies that it really connects IM1 and products of PhOC(O)H+$SO_2$ (P3). The formation of PhOC(O)H is a new product channel that has not been discussed in other similar CIs+$SO_2$ reactions.

In addition to three direct reaction pathways, IM1 can also isomerize to another intermediate IM3 via ring opening transition state TSIM1-3, with a lower barrier of 96.75 kJ/mol. In TSIM1-3, the breaking O1-O2 bond is 1.976 Å. Subsequently, three reaction pathways of IM3 will be open. As shown in Figure 1, the most feasible reaction pathways of IM3 is the formation of P1 via TSIM3-P1. TSIM3-P1 is 54.11 kJ/mol lower in energy than the initial reactants and the barrier height of it is only 32.02 kJ/mol.

As discussed above, the singlet bisoxy diradical PhC(H)O(O) cannot be produced directly from IM1, whereas, via TSIM3-P4, the products of PhC(H)O(O)+$SO_2$ (P4) will be formed starting from IM3 by surmounting a barrier of 41.60 kJ/mol. It is worth noting that TSIM3-P4 lies above TSIM3-P1 by about 10 kJ/mol. Moreover, the reaction from IM3 to P4 is endergonic, and the process is reversible, so we can conclude that P4 would never be formed in the reaction.

The third reaction pathway of IM3 is the formation of PhC(O)$OSO_2$+H (P5) via C1-H bond rupture transition state TSIM3-P5. The barrier height of TSIM3-P5 is 66.26 kJ/mol, and apparently the formation of P5 is not competitive with that of P1 initiated from IM3, due to it being the highest barrier.

As can be seen from Figure 1, because of the level of the lowest barrier, the formation of P1 through indirect reaction processes, viz. IM1→TSIM1-3→IM3→TS3-P1→P1 is more favorable than that through direct reaction pathway, and is the major product channel, and our calculational result is consistent with the conclusion that the reaction of CI+$SO_2$ is surprisingly contributive to the formation of atmospheric $H_2SO_4$ [3]. As for the formation of PhCOOH+$SO_2$ (P2), although it is the most favored product channel thermodynamically, the highest barrier height makes this pathway infeasible from IM1.

Similar to IM1, both the direct and indirect reaction pathways of IM2 have been considered, and they are depicted in Figure 2.

The product pathway of IM2 for the formation of P1 has been studied firstly, whereas no right transition state has been located at the B3LYP level. The search for such structure results in the transition state connecting the intermediate formed between *syn*-PhCHOO with $SO_2$ and P1.

Starting from IM2, the PhCOOH+$SO_2$ (P2) will be formed via TSIM2-P2 with a barrier of 113.32 kJ/mol. As shown in Figure 2, TSIM2-P2 is 15.81 kJ/mol lower in energy than that TSIM1-P2, and this indicates that the formation of P2 via TSIM2-P2 is more feasible. As for the production of P3 from IM2, the transition state TSIM2-P3 involves the highest barrier of 144.32 kJ/mol, thus, the contribution from this product channel can be negligible.

With the fracture of O1-O2 bond, the intermediate IM4 will be formed via TSIM2-4 with a barrier height of 111.38 kJ/mol. IM4 has similar reaction pathways to IM3, viz. the formation of P1, P4, and P5 via TSIM4-P1, TSIM4-P4, and TSIM4-P5, respectively. The relative energies of TSIM4-P1, TSIM4-P4, and TSIM4-P5 are −55.89, −49.29 and −26.46 kJ/mol, respectively. Similar to the reaction from IM3 to P4, the formation of P4 and P5 starting from IM4 can be almost ruled out, since these two pathways are not favorable thermodynamically, and are dynamically compared with the formation of P1 from IM4. As a result, P1 and P2 formed through TSIM4-P1 and TSIM2-P2 are the major and minor products of IM2, respectively.

Comparing Figure 1 with Figure 2, we can see that from both IM1 and IM2, the formation of P1 via indirect reaction pathways is the main product channels. IM1 and IM2 are a pair of isomers with similar structures and closer energies, however, due to their different spatial conformation, the energy of TSIM1-3 is 17.46 kJ/mol lower than that of TSIM2-4, which results in the formation of P1 starting from IM1 to be more feasible, that is to say, IM1 and IM2 have the conformation-dependent reactivity. Moreover, the formation of P2 from IM2 may also have slight contribution to the final product distribution, based on our calculations. In the experiment, besides the dominant $SO_3$, no other possible products have been given [14]. Fortunately, our theoretical prediction for the possible product distribution of the title reaction is consistent with the similar reaction of $CH_2OO$+$SO_2$ [24]. In addition, we can see that during the formation of P1 via indirect reaction pathways of IM1, all the transition states lie below the initial reactants by about 50 kJ/mol, which suggests that the reaction of *anti*-PhCHOO+$SO_2$ will be fast. This is attributed to the fact that the effective activation energy $\Delta E_{\text{eff}}^{\neq}$ ($\Delta E_{\text{eff}}^{\neq} = E^{\text{TS}} - E^{\text{Reactants}}$) [49,50] for the rate-determining step transition state TSIM1-3 is negative. A negative $\Delta E_{\text{eff}}^{\neq}$ is crucial to the reaction activity and product distribution [51,52]. Nevertheless, this behavior will be testified by further kinetic investigation (see next section).

### 3.2. Kinetic Calculation

The rate constant for the reaction of $SO_2$ with the Criegee intermediate can be estimated in terms of the steady state approximation [21] for the IM1 adduct:

$$\frac{d[\text{IM1}]}{dt} = k_{\text{cap}}[\text{SO}_2][anti-\text{PhCHOO}] - k_{\text{diss},1}[\text{IM1}] - k_{\text{TSIM1-3}}[\text{IM1}] - k_{\text{TSIM1-P1}}[\text{IM1}] - k_{\text{TSIM1-P2}}[\text{IM1}] - k_{\text{TSIM1-P3}}[\text{IM1}] = 0 \quad (1)$$

$$[\text{IM1}] = \frac{k_{\text{cap}}[\text{SO}_2][anti-\text{PhCHOO}]}{k_{\text{diss},1} + k_{\text{TSIM1-3}} + k_{\text{TSIM1-P1}} + k_{\text{TSIM1-P2}} + k_{\text{TSIM1-P3}}} \quad (2)$$

Then, the reaction rate starting from IM1 can be represented as:

$$r = k_{\text{TSIM1-3}}\,[\text{IM1}] = \frac{k_{\text{TSIM1-3}}\,k_{\text{cap}}[\text{SO}_2][anti-\text{PhCHOO}]}{k_{\text{diss},1}+k_{\text{TSIM1-3}}+k_{\text{TSIM1-P1}}+k_{\text{TSIM1-P2}}+k_{\text{TSIM1-P3}}} = k_1\,[\text{SO}_2][anti-\text{PhCHOO}] \quad (3)$$

Therefore, the rate constant $k_1$ can be expressed as:

$$k_1 = \frac{k_{\text{TSIM1-3}} \times k_{\text{cap}}}{k_{\text{diss},1} + k_{\text{TSIM1-3}} + k_{\text{TSIM1-P1}} + k_{\text{TSIM1-P2}} + k_{\text{TSIM1-P3}}} \quad (4)$$

where $k_{\text{cap}}$ represents the capture rate constant between $SO_2$ and *anti*-PhCHOO that form the IM1 adduct, $k_{\text{diss},1}$ stands for the rate constant for the IM1 adduct dissociates back to the reactants, and

$k_{\text{TSIM1-3}}$, $k_{\text{TSIM1-P1}}$, $k_{\text{TSIM1-P2}}$ and $k_{\text{TSIM1-P3}}$ are the unimolecular rate constants of the dissociation or isomerization channels of the IM1 adduct, and they can be calculated using transition state theory (TST) [53–55]:

$$k_{uni} = \Gamma \frac{k_B T}{h} \frac{Q_{TS}}{Q_{IM1}} exp(-\frac{E_{TS} - E_{IM1}}{RT}) \quad (5)$$

where $Q$ represents the partition functions of the respective subscripted species, while $E$ are the zero-point corrected total energies of the respective subscripted species. $\Gamma$ denotes the Wigner's tunneling correction [56]. $k_B$, $h$, $T$, and $R$ represent Boltzmann's constant ($1.38 \times 10^{-23}$ J $K^{-1}$), Planck's constant ($6.63 \times 10^{-34}$ J·s), the absolute temperature, and the ideal gas constant (8.314 J $mol^{-1}$ $K^{-1}$), respectively.

As stated above, the formation of IM1 and IM2 is barrierless. The capture rate constant $k_{\text{cap}}$ can be calculated using the long-range variational TST expression derived by Georgievskii and Klippenstein [57], which can be written as:

$$k_{cap} = \frac{C(d_1 d_2)^{2/3}}{\mu^{1/2} T^{1/6}} \quad (6)$$

where $d_1$ and $d_2$ are the dipole moments of the $SO_2$ and *anti*-PhCHOO, $\mu$ is the reduced mass of the *anti*-PhCHOO–$SO_2$ collision, $T$ is the absolute temperature, and $C$ is a constant of proportionality whose value is 5.87 [57] for the dipole-dipole interaction between two nonlinear molecules.

The value of $k_{\text{cap}}$ for the IM1 adduct at 298 K was found to be $6.02 \times 10^{-10}$ $cm^3$ $molecule^{-1}$ $s^{-1}$ by using the dipole of *anti*-PhCHOO and $SO_2$ (6.5619 D and 2.0269 D at the B3LYP/6-311++G(d,p) level of theory). This value is similar to that obtained in barrierless $CH_2OO$-$SO_2$ association study [24]. From elementary TST, and using the B3LYP-determined moments of inertia, and the B3LYP-determined vibrational frequencies and the zero-point-corrected CCSD(T) electronic energies, we obtain the following unimolecular rate constants: $k_{\text{diss,1}} = 4.87 \times 10^{-7}$ $s^{-1}$, $k_{\text{TSIM1-3}} = 1.08 \times 10^{-4}$ $s^{-1}$, $k_{\text{TSIM1-P1}} = 4.12 \times 10^{-7}$ $s^{-1}$, $k_{\text{TSIM1-P2}} = 1.50 \times 10^{-10}$ $s^{-1}$, $k_{\text{TSIM1-P3}} = 5.25 \times 10^{-10}$ $s^{-1}$ at 298 K. Thus, the rate constant $k_1$ is computed to be $5.99 \times 10^{-10}$ $cm^3$ $molecule^{-1}$ $s^{-1}$.

By following a similar procedure, the rate constant $k_2$ for the IM2 adduct can also be obtained as follows:

$$k_2 = \frac{k_{\text{TSIM2-4}} \times k_{\text{cap}}}{k_{\text{diss,2}} + k_{\text{TSIM2-4}} + k_{\text{TSIM2-P2}} + k_{\text{TSIM2-P3}}} \quad (7)$$

The unimolecular rate constants beginning with IM2 at 298 K were computed to be $k_{\text{diss,2}} = 1.65 \times 10^{-6}$ $s^{-1}$, $k_{\text{TSIM2-4}} = 3.58 \times 10^{-7}$ $s^{-1}$, $k_{\text{TSIM2-P2}} = 1.73 \times 10^{-7}$ $s^{-1}$, $k_{\text{TSIM2-P3}} = 3.29 \times 10^{-13}$ $s^{-1}$, respectively. As a result, the computed value for the rate constant $k_2$ at 298 K is $9.94 \times 10^{-11}$ $cm^3$ $molecule^{-1}$ $s^{-1}$.

Finally, the overall bimolecular rate constant for the *anti*-PhCHOO+$SO_2$ reaction was determined to be $6.98 \times 10^{-10}$ $cm^3$ $molecule^{-1}$ $s^{-1}$ by adding up the individual bimolecular rate constant $k_1$ and $k_2$.

There are no experimental data about the bimolecular rate constant for the *anti*-PhCHOO + $SO_2$ reaction. Information on the bimolecular rate constant in the reactions of $SO_2$ with Criegee intermediates is available in the case of $CH_2OO$ and $(CH_3)_2COO$ [3,21]. Our calculated value matches within 1 order of magnitude compared with the experimental value of $(3.9 \pm 0.7) \times 10^{-11}$ $cm^3$ $molecule^{-1}$ $s^{-1}$ for the $CH_2OO$+$SO_2$ reaction recommended by Welz et al. [3]. Moreover, the obtained rate constant presented here agrees well with the computed value of $4 \times 10^{-10}$ $cm^3$ $molecule^{-1}$ $s^{-1}$ for both the $CH_2OO$+$SO_2$ and the $(CH_3)_2COO$+$SO_2$ oxidation reactions reported by Kurtén et al. [21].

## 4. Conclusions

Quantum chemical calculations have been performed to characterize the potential energy surface of the *anti*-PhCHOO+$SO_2$ reaction at the UCCSD(T)/6-311++G(d,p) level of energy calculations based on UB3LYP/6-311++G(d,p) optimized geometries together with ZPE corrections. Various possible

reaction pathways have been probed. The calculated results show that the reaction begins with the formation of two reactant complexes RC1 and RC2 and produces two energy-rich adducts IM1 and IM2 barrierlessly in the process of $SO_2$ association with *anti*-PhCHOO from different directions. IM1 and IM2 are a pair of isomers with similar structures and closer energies, however, IM1 shows higher reactivity than that IM2 in the formation of the most favorable product of P1 via indirect reaction pathways, which suggests the conformation-dependent reactivity of *anti*-PhCHOO with $SO_2$. P2 is found to be the less competitive product, followed by the almost negligible products of P3, P4 and P5. Based on the quantum chemical calculations and transition state theory, the overall reaction rate constant is predicted to be $6.98 \times 10^{-10}$ $cm^3$ $molecule^{-1}$ $s^{-1}$ at 298 K, which is in agreement with the similar $CH_2OO+SO_2$ and $(CH_3)_2COO+SO_2$ reactions.

**Supplementary Materials:** Figure S1: Optimized geometries of species including reactants, reactant complexes, transition states and intermediates involved in the reaction of *anti*-PhCHOO+$SO_2$ at the UB3LYP/6-311++G(d,p) level. Figure S2: Optimized geometries of various species involved in the subsequent reaction pathways of IM1 at the UB3LYP/6-311++G(d,p) level. Figure S3: Optimized geometries of various species involved in the subsequent reaction pathways of IM2 at the UB3LYP/6-311++G(d,p) level. Figure S4: The intrinsic reaction coordinate of TSIM1-P3. Table S1: The total energies (hartree) obtained at the UCCSD(T)//UB3LYP and UCCSD//UB3LYP levels of theory together with the %TAE(T) of various species in the reaction of *anti*-PhCHOO+$SO_2$. Table S2: The ZPE (hartree), total energies (E, hartree) and relative energies (ΔE, Δ(E+ZPE), kJ/mol) without and with ZPE corrections of various species calculated at the UCCSD(T)//UB3LYP levels of theory in the reaction of *anti*-PhCHOO+$SO_2$. Cartesian coordinates for all optimized structures at the UB3LYP/6-311++G(d,p) and UBH&HLYP/6-311++G(d,p) levels of theory.

**Author Contributions:** Conceptualization, B.D.; Methodology, B.D. and W.Z.; Software, W.Z.; Validation, B.D. and W.Z.; Formal Analysis, W.Z.; Investigation, B.D. and W.Z.; Resources, B.D.; Data Curation, B.D. and W.Z.; Writing-Original Draft Preparation, B.D. and W.Z.; Writing-Review & Editing, W.Z.; Visualization, W.Z.; Supervision, W.Z.; Project Administration, W.Z.; Funding Acquisition, B.D. All authors have read and agreed to the published version of the manuscript.

**Funding:** This work was supported by the Doctoral Scientific Research Foundation of Jiangsu Normal University (Grant No. 13XLR003).

**Acknowledgments:** The authors would like to acknowledge the support of the Top-notch Academic Programs Project of Jiangsu Higher Education Institutions (TAPP).

**Conflicts of Interest:** The authors declare no conflict of interest.

## References

1. Su, Y.T.; Huang, Y.H.; Witek, H.A.; Lee, Y.P. Infrared Absorption Spectrum of the Simplest Criegee Intermediate $CH_2OO$. *Science* **2013**, *340*, 174–176. [CrossRef]
2. Taatjes, C.A.; Meloni, G.; Selby, T.M.; Trevitt, A.J.; Osborn, D.L.; Percival, C.J.; Shallcross, D.E. Direct Observation of the Gas-Phase Criegee Intermediate ($CH_2OO$). *J. Am. Chem. Soc.* **2008**, *130*, 11883–11885. [CrossRef] [PubMed]
3. Welz, O.; Savee, J.D.; Osborn, D.L.; Vasu, S.S.; Percival, C.J.; Shallcross, D.E.; Taatjes, C.A. Direct Kinetic Measurements of Criegee Intermediate ($CH_2OO$) Formed by Reaction of $CH_2I$ with $O_2$. *Science* **2012**, *335*, 204–207. [CrossRef]
4. Kjaergaard, H.G.; Kurtén, T.; Nielsen, L.B.; Jørgensen, S.; Wennberg, P.O. Criegee Intermediates React with Ozone. *J. Phys. Chem. Lett.* **2013**, *4*, 2525–2529. [CrossRef]
5. Aplincourt, P.; Ruiz-López, M.F. Theoretical Investigation of Reaction Mechanisms for Carboxylic Acid Formation in the Atmosphere. *J. Am. Chem. Soc.* **2000**, *122*, 8990–8997. [CrossRef]
6. Fenske, J.D.; Hasson, A.S.; Ho, A.W.; Paulson, S.E. Measurement of Absolute Unimolecular and Bimolecular Rate Constants for $CH_3CHOO$ Generated by the *trans*-2-Butene Reaction with Ozone in the Gas Phase. *J. Phys. Chem. A* **2000**, *104*, 9921–9932. [CrossRef]
7. Ryzhkov, A.B.; Ariya, P.A. The Importance of Water Clusters $(H_2O)n$ (n = 2,...,4) in the Reaction of Criegee Intermediate with Water in the Atmosphere. *Chem. Phys. Lett.* **2006**, *419*, 479–485. [CrossRef]
8. Anglada, J.M.; González, J.; Torrent-Sucarrat, M. Effects of the Substituents on the Reactivity of Carbonyl Oxides. A Theoretical Study on the Reaction of Substituted Carbonyl Oxides with Water. *Phys. Chem. Chem. Phys.* **2011**, *13*, 13034–13035. [CrossRef]

9. Berndt, T.; Voigtländer, J.; Stratmann, F.; Junninen, H.; Mauldin, R.L., III; Sipilä, M.; Kulmala, M.; Herrmann, H. Competing Atmospheric Reactions of $CH_2OO$ with $SO_2$ and Water Vapour. *Phys. Chem. Chem. Phys.* **2014**, *16*, 19130–19136. [CrossRef]
10. Stone, D.; Blitz, M.; Daubney, L.; Howes, N.U.M.; Seakins, P. Kinetics of $CH_2OO$ Reactions with $SO_2$, $NO_2$, NO, $H_2O$ and $CH_3CHO$ as a Function of Pressure. *Phys. Chem. Chem. Phys.* **2014**, *16*, 1139–1149. [CrossRef]
11. Newland, M.J.; Rickard, A.R.; Alam, M.S.; Vereecken, L.; Munoz, A.; Ródenas, M.; Bloss, W.J. Kinetics of Stabilized Criegee Intermediates Derived from Alkene Ozonolysis: Reactions with $SO_2$, $H_2O$ and Decomposition under Boundary Layer Conditions. *Phys. Chem. Chem. Phys.* **2015**, *17*, 4076–4088. [CrossRef] [PubMed]
12. Chao, W.; Hsieh, J.-T.; Chang, C.-H.; Lin, J.J.-M. Direct Kinetic Measurement of the Reaction of the Simplest Criegee Intermediate with Water Vapor. *Science* **2015**, *347*, 751–754. [CrossRef] [PubMed]
13. Long, B.; Bao, J.L.; Truhlar, D.G. Atmospheric Chemistry of Criegee Intermediates. Unimolecular Reactions and Reactions with Water. *J. Am. Chem. Soc.* **2016**, *138*, 14409–14422. [CrossRef]
14. Díaz-de-Mera, Y.; Aranda, A.; Martínez, E.; Rodríguez, A.A.; Rodríguez, D.; Rodríguez, A. Formation of Secondary Aerosols from the Ozonolysis of Styrene: Effect of $SO_2$ and $H_2O$. *Atmos. Environ.* **2017**, *171*, 25–31. [CrossRef]
15. Long, B.; Tan, X.F.; Long, Z.W.; Wang, Y.B.; Ren, D.S.; Zhang, W.J. Theoretical Studies on Reactions of the Stabilized $H_2COO$ with $HO_2$ and the $HO_2\cdots H_2O$ Complex. *J. Phys. Chem. A* **2011**, *115*, 6559–6567. [CrossRef] [PubMed]
16. Chen, L.; Huang, Y.; Xue, Y.G.; Cao, J.J.; Wang, W.L. Competition between $HO_2$ and $H_2O_2$ Reactions with $CH_2OO$/*anti*-$CH_3CHOO$ in the Oligomer Formation: A Theoretical Perspective. *J. Phys. Chem. A* **2017**, *121*, 6981–6991. [CrossRef]
17. Ouyang, B.; McLeod, M.W.; Jones, R.L.; Bloss, W.J. $NO_3$ Radical Production from the Reaction between the Criegee Intermediate $CH_2OO$ and $NO_2$. *Phys. Chem. Chem. Phys.* **2013**, *15*, 17070–17075. [CrossRef]
18. Vereecken, L.; Nguyen, H.M.T. Theoretical Study of the Reaction of Carbonyl Oxide with Nitrogen Dioxide: $CH_2OO + NO_2$. *Int. J. Chem. Kinet.* **2017**, *49*, 752–760. [CrossRef]
19. Chhantyal-Pun, R.; Welz, O.; Savee, J.D.; Eskola, A.J.; Lee, E.P.F.; Blacker, L.; Hill, H.R.; Ashcroft, M.; Khan, M.A.H.; Lloyd-Jones, G.C.; et al. Direct Measurements of Unimolecular and Bimolecular Reaction Kinetics of the Criegee Intermediate $(CH_3)_2COO$. *J. Phys. Chem. A* **2017**, *121*, 4–15. [CrossRef]
20. Jiang, L.; Xu, Y.S.; Ding, A.Z. Reaction of Stabilized Criegee Intermediates from Ozonolysis of Limonene with Sulfur Dioxide: Ab Initio and DFT Study. *J. Phys. Chem. A* **2010**, *114*, 12452–12461. [CrossRef]
21. Kurtén, T.; Lane, J.R.; Jørgensen, S.; Kjaergaard, H.G. A Computational Study of the Oxidation of $SO_2$ to $SO_3$ by Gas-Phase Organic Oxidants. *J. Phys. Chem. A* **2011**, *115*, 8669–8681. [CrossRef] [PubMed]
22. Berndt, T.; Jokinen, T.; Mauldin, R.L., III; Petäjä, T.; Herrmann, H.; Junninen, H.; Paasonen, P.; Worsnop, D.R.; Sipilä, M. Gas-Phase Ozonolysis of Selected Olefins: The Yield of Stabilized Criegee Intermediate and the Reactivity toward $SO_2$. *J. Phys. Chem. Lett.* **2012**, *3*, 2892–2896. [CrossRef]
23. Vereecken, L.; Harder, H.; Novelli, A. The Reaction of Criegee Intermediates with NO, $RO_2$, and $SO_2$, and Their Fate in the Atmosphere. *Phys. Chem. Chem. Phys.* **2012**, *14*, 14682–14695. [CrossRef] [PubMed]
24. Kuwata, K.T.; Guinn, E.J.; Hermes, M.R.; Fernandez, J.A.; Mathison, J.M.; Huang, K. A Computational Re-examination of the Criegee Intermediate–Sulfur Dioxide Reaction. *J. Phys. Chem. A* **2015**, *119*, 10316–10335. [CrossRef] [PubMed]
25. Liu, Y.Q.; Liu, F.H.; Liu, S.Y.; Dai, D.X.; Dong, W.R.; Yang, X.M. A Kinetic Study of the $CH_2OO$ Criegee Intermediate Reaction with $SO_2$, $(H_2O)_2$, $CH_2I_2$ and I Atoms using OH Laser Induced Fluorescence. *Phys. Chem. Chem. Phys.* **2017**, *19*, 20786–20794. [CrossRef]
26. Taatjes, C.A.; Welz, O.; Eskola, A.J.; Savee, J.D.; Scheer, A.M.; Shallcross, D.E.; Rotavera, B.; Lee, E.P.F.; Dyke, J.M.; Mok, D.K.W.; et al. Direct Measurements of Conformer-Dependent Reactivity of the Criegee Intermediate $CH_3CHOO$. *Science* **2013**, *340*, 177–180. [CrossRef]
27. Berndt, T.; Jokinen, T.; Sipilä, M.; Mauldin, R.L., III; Herrmann, H.; Stratmann, F.; Junninen, H.; Kulmala, M. $H_2SO_4$ Formation from the Gas-Phase Reaction of Stabilized Criegee Intermediates with $SO_2$: Influence of Water Vapour Content and Temperature. *Atmos. Environ.* **2014**, *89*, 603–612. [CrossRef]
28. Lin, H.-Y.; Huang, Y.-H.; Wang, X.; Bowman, J.M.; Nishimura, Y.; Witek, H.A.; Lee, Y.-P. Infrared Identification of the Criegee Intermediates *syn*- and *anti*-$CH_3CHOO$, and Their Distinct Conformation-Dependent Reactivity. *Nat. Commun.* **2015**, *6*, 7012–7018. [CrossRef]

29. Boy, M.; Mogensen, D.; Smolander, S.; Zhou, L.; Nieminen, T.; Paasonen, P.; Plass-Dülmer, C.; Sipilä, M.; Petäjä, T.; Mauldin, L.; et al. Oxidation of $SO_2$ by Stabilized Criegee Intermediate (sCI) Radicals as a Crucial Source for Atmospheric Sulfuric Acid Concentrations. *Atmos. Chem. Phys.* **2013**, *13*, 3865–3879. [CrossRef]
30. Saheb, V.; Nazari, A. The Reaction of OH Radical with the Criegee Intermediate Propanone Oxide: Theoretical Investigations. *Comput. Theor. Chem.* **2020**, *1175*, 112726. [CrossRef]
31. Cai, J.; Lu, Y.S.; Wang, W.N.; Chen, L.; Liu, F.Y.; Wang, W.L. Reaction Mechanism and Kinetics of Criegee Intermediate $CH_2OO$ with $CH_2$=C($CH_3$)CHO. *Comput. Theor. Chem.* **2019**, *1170*, 112644. [CrossRef]
32. Mauldin, R.L., III; Berndt, T.; Sipilä, M.; Paasonen, P.; Petäjä, T.; Kim, S.; Kurten, T.; Stratmann, F.; Kerminen, V.M.; Kulmala, M. A New Atmospherically Relevant Oxidant of Sulphur Dioxide. *Nature* **2012**, *488*, 193–196. [CrossRef] [PubMed]
33. Ehn, M.; Thornton, J.A.; Kleist, E.; Sipilä, M.; Junninen, J.; Pullinen, I.; Springer, M.; Rubach, F.; Tillmann, R.; Lee, B.; et al. A Large Source of Low-Volatility Secondary Organic Aerosol. *Nature* **2014**, *506*, 476–479. [CrossRef] [PubMed]
34. Berresheim, H.; Adam, M.; Monahan, C.; O'Dowd, C.; Plane, J.M.C.; Bohn, B.; Rohrer, F. Missing $SO_2$ Oxidant in the Coastal Atmosphere?–Observations from High-Resolution Measurements of OH and Atmospheric Sulfur Compounds. *Atmos. Chem. Phys.* **2014**, *14*, 12209–12223. [CrossRef]
35. Sarwar, G.; Simon, H.; Fahey, K.; Mathur, R.; Goliff, W.; Stockwell, W. Impact of Sulfur Dioxide Oxidation by Stabilized Criegee Intermediate on Sulfate. *Atmos. Environ.* **2014**, *85*, 204–214. [CrossRef]
36. Frisch, M.J.; Trucks, G.W.; Schlegel, H.B.; Scuseria, G.E.; Robb, M.A.; Cheeseman, J.R.; Scalmani, G.; Barone, V.; Mennucci, B.; Petersson, G.A.; et al. *Gaussian 09, Revision, D.01*; Gaussian Inc.: Wallingford, CT, USA, 2013.
37. Becke, A.D. Density-Functional Exchange-Energy Approximation with Correct Asymptotic Behavior. *Phys. Rev. A* **1988**, *38*, 3098–3100. [CrossRef]
38. Lee, C.; Yang, W.; Parr, R.G. Development of the Colle-Salvetti Correlation-Energy Formula into a Functional of the Electron Density. *Phys. Rev. B: Condens. Matter Mater. Phys.* **1988**, *37*, 785–789. [CrossRef] [PubMed]
39. Gonzalez, C.; Schlegel, H.B. An Improved Algorithm for Reaction Path Following. *J. Chem. Phys.* **1989**, *90*, 2154–2161. [CrossRef]
40. Gonzalez, C.; Schlegel, H.B. Reaction Path Following in Mass-Weighted Internal Coordinates. *J. Phys. Chem.* **1990**, *94*, 5523–5527. [CrossRef]
41. Pople, J.A.; Head-Gordon, M.; Raghavachari, K. Quadratic Configuration Interaction. A General Technique for Determining Electron Correlation Energies. *J. Chem. Phys.* **1987**, *87*, 5968–5975. [CrossRef]
42. Merrick, J.P.; Moran, D.; Radom, L. An Evaluation of Harmonic Vibrational Frequency Scale Factors. *J. Phys. Chem. A* **2007**, *111*, 11683–11700. [CrossRef] [PubMed]
43. Becke, A.D. A New Mixing of Hartree–Fock and Local Density-Functional Theories. *J. Chem. Phys.* **1993**, *98*, 1372–1377. [CrossRef]
44. Raghunath, P.; Lee, Y.-P.; Lin, M.C. Computational Chemical Kinetics for the Reaction of Criegee Intermediate $CH_2OO$ with $HNO_3$ and Its Catalytic Conversion to OH and HCO. *J. Phys. Chem. A* **2017**, *121*, 3871–3878. [CrossRef] [PubMed]
45. Wei, W.M.; Zheng, R.H.; Pan, Y.L.; Wu, Y.K.; Yang, F.; Hong, S. Ozone Dissociation to Oxygen Affected by Criegee Intermediate. *J. Phys. Chem. A* **2014**, *118*, 1644–1650. [CrossRef]
46. Noodleman, L. Valence Bond Description of Antiferromagnetic Coupling in Transition Metal Dimers. *J. Chem. Phys.* **1981**, *74*, 5737–5743. [CrossRef]
47. Karton, A.; Rabinovich, E.; Martin, J.M.L.; Ruscic, B. W4 Theory for Computational Thermochemistry: In Pursuit of Confident Sub-kJ/mol Predictions. *J. Chem. Phys.* **2006**, *125*, 144108–144125. [CrossRef]
48. Karton, A. A Computational Chemist's Guide to Accurate Thermochemistry for Organic Molecules. *WIREs Comput. Mol. Sci.* **2016**, *6*, 292–310. [CrossRef]
49. Iuga, C.; Alvarez-Idaboy, J.R.; Reyes, L.; Vivier-Bunge, A. Can a Single Water Molecule Really Catalyze the Acetaldehyde + OH Reaction in Tropospheric Conditions? *J. Phys. Chem. Lett.* **2010**, *1*, 3112–3115. [CrossRef]
50. Iuga, C.; Alvarez-Idaboy, J.R.; Vivier-Bunge, A. On the Possible Catalytic Role of a Single Water Molecule in the Acetone + OH Gas Phase Reaction: A Theoretical Pseudo-second-order Kinetics Study. *Theor. Chem. Acc.* **2011**, *129*, 209–217. [CrossRef]
51. Asatryan, R.; da Silva, G.; Bozzelli, J.W. Quantum Chemical Study of the Acrolein ($CH_2CHCHO$) + OH + $O_2$ Reactions. *J. Phys. Chem. A* **2010**, *114*, 8302–8311. [CrossRef]

52. da Silva, G. Reaction of Methacrolein with the Hydroxyl Radical in Air: Incorporation of Secondary $O_2$ Addition into the MACR + OH Master Equation. *J. Phys. Chem. A* **2012**, *116*, 5317–5324. [CrossRef]
53. Pilling, M.J.; Seakins, P.W. *Reaction Kinetics*; Oxford University Press Inc.: New York, NY, USA, 1999.
54. Li, J.Y.; Tsona, N.T.; Du, L. The Role of $(H_2O)_{1\text{-}2}$ in the $CH_2O$ + ClO Gas-Phase Reaction. *Molecules* **2018**, *23*, 2240. [CrossRef] [PubMed]
55. Cheng, N.S.; Gan, Q.; Yu, Q.; Zhang, X.M.; Li, R.; Qian, S.C.; Feng, C.G. Initial Mechanisms for the Unimolecular Thermal Decomposition of 2,6-Diamino-3,5-dinitropyrazine-1-oxide. *Molecules* **2019**, *24*, 125. [CrossRef] [PubMed]
56. Wigner, E. Calculation of the Rate of Elementary Association Reactions. *J. Chem. Phys.* **1937**, *5*, 720–725. [CrossRef]
57. Georgievskii, Y.; Klippenstein, S.J. Long-Range Transition State Theory. *J. Chem. Phys.* **2005**, *122*, 194103–194117. [CrossRef]


**Sample Availability:** Samples of the compounds are available from the authors.